

# Passive Shunt Damping of a Piezoelectric Stack Nanopositioner

Arnfinn Aas Eielsen and Andrew J. Fleming

**Abstract**—The speed and accuracy of nanopositioning systems is heavily influenced by the presence of lightly damped mechanical resonances. In this work, an electrical impedance is connected in series with the driving piezoelectric stack actuator to damp the first mechanical resonance. The electrical shunt is shown to act equivalently to an output feedback controller except that no sensor is required. A simple inductor-resistor shunt circuit is demonstrated to damp the first mechanical resonance of a high-speed nanopositioner by 19.6 dB. The technique of shunt damping is low-cost, simple, guaranteed to be stable, and significantly improves the system response.

## I. INTRODUCTION

Nanopositioning devices generate fine mechanical displacement with resolution down to atomic scale [1]. Applications include the alignment of optical fibers [2], optical beam pointing [3], positioning in Scanning Probe Microscopes (SPMs) [1], [4], and nanofabrication [5].

Due to their effectively infinite resolution, piezoelectric actuators are universally employed in nanopositioning devices. Unfortunately the accuracy of nanopositioning platforms is significantly degraded by creep and hysteresis exhibited by most piezoelectric materials. In addition, low-frequency mechanical resonances cause oscillation and degrade the performance of controllers designed to reduce nonlinearity [1].

To avoid excitation of the mechanical resonance in open-loop, the frequency of driving signals is limited to between 1% and 10% of the resonance frequency (depending on the signal). In the case of scanning motion the driving signal is typically a triangle wave, comprised of odd harmonics of the fundamental frequency. If these harmonics excite one or more resonant modes, the resulting displacement can become highly oscillatory. This is a major limitation for applications that require high-speed positioning such as video speed microscopy [6]–[9].

The transient response of nanopositioners can be drastically improved by damping the first mechanical resonance. A number of techniques for damping control have been demonstrated successfully in the literature, these include Positive Position Feedback (PPF) [10], polynomial based control [11], shunt control [12], [13], resonant control [14] and Integral Resonant Control (IRC) [15]–[17].

In this paper we describe a new technique for damping mechanical resonances in stack actuated nanopositioners. By connecting an electrical impedance in series with the stack actuator, the impedance can be designed to damp a single, or

This work was supported by the Norwegian Research Council and the Norwegian University of Science and Technology. Experiments were performed at the Laboratory for Dynamics and Control of Nanosystems.

Andrew J. Fleming [andrew.fleming@newcastle.edu.au](mailto:andrew.fleming@newcastle.edu.au) is with the School of Electrical Engineering and Computer Science at the University of Newcastle, Callaghan, NSW, Australia

Arnfinn Aas Eielsen [eielsen@itk.ntnu.no](mailto:eielsen@itk.ntnu.no) is with the Department of Engineering Cybernetics at the Norwegian University of Science and Technology, Trondheim, Norway

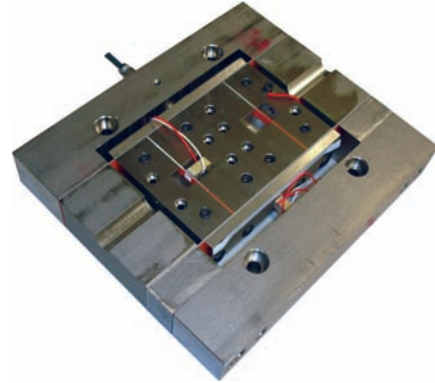


Fig. 1. High-speed nanopositioning platform described in [18].

multiple mechanical modes. This technique, known as shunt damping [13], was first applied to piezoelectric tube scanners in reference [12]. In that work, the shunt was implemented electronically and placed in parallel with the stack actuator and a driving charge source. In this work, it is demonstrated that a standard voltage amplifier in series with an inductor and resistor can be used to achieve the same result.

In the following section, an electromechanical model of a nanopositioning platform is developed. The shunt circuit is then shown to act equivalently to an output feedback controller. That is, it is possible to convert any output feedback controller to a shunt circuit and vice-versa. However, this may not be desirable as there is no guarantee that the resulting controller, or shunt circuit, will be causal or stable. The shunt circuit used in this work is a simple inductor and resistor, this acts analogously to a tuned mechanical absorber. In Section III the shunt circuit is applied experimentally. Results demonstrate an excellent agreement between theoretical and experimental responses. The first mechanical resonance is reduced by 19.6 dB which significantly improves the nanopositioner's transient response with negligible increases in cost, complexity, and noise.

## II. MODELING

### A. Description of the experimental system

In [18] a high-bandwidth lateral nanopositioning platform was designed for video speed scanning probe microscopy. This device, pictured in Fig. 1, is a serial kinematic device with two moving platforms both suspended by leaf flexures and driven directly by 10 mm Noliac SCMAP07 stack actuators. The displacement was measured using an ADE Tech 4810 gage with an ADE Tech 2805 probe (10  $\mu\text{m/V}$ ). The actuator was driven with a Piezodrive PDL200 linear voltage amplifier. Only the axis with the lowest resonance frequency was used in this work.

### B. Stack actuator blocking force

The actuator used is a piezoelectric stack. It consists of multiple layers of piezoelectric ceramic material. The stack is designed so that applied electric field is in parallel to the poling direction of the ceramic. This causes the developed force to work on the attached mechanical structure in the same direction.

The blocking force of the actuator can be found by assuming that the stack is clamped in the poling direction, but free to expand in other directions. All forces are also assumed to be working along the poling direction, as well as the applied electric field. Under these conditions the stress on one layer, or element, of the stack will be

$$\sigma_3 = -d_{33} (c_{33}^E - 2c_{13}^E \nu) E_3, \quad \nu = \frac{c_{13}^E}{c_{11}^E + c_{12}^E}.$$

The poling direction is along the 3 axis.  $\sigma_3$  is the stress [N/m<sup>2</sup>] in this direction,  $d_{33}$  is the piezoelectric strain constant [m/V] for the material in this direction,  $c_{11}^E$ ,  $c_{12}^E$ ,  $c_{13}^E$ , and  $c_{33}^E$  are elastic stiffnesses [N/m<sup>2</sup>] for the material, and  $E_3$  is the applied electric field [V/m].

The geometry of one stack element should be well approximated by a rectangular cuboid, with length, or thickness,  $t$ , and having a surface area of  $A$  for the faces normal to the direction of the length. Any forces working on the attached mechanical structure should be distributed over these faces, and any voltage applied over electrodes on these faces, must be distributed over the thickness. The stress on the element due to a force  $F_a$  in the poling direction should therefore be  $\sigma_3 = \frac{F_a}{A}$ , and the electric field due to applied voltage  $V_a$  should be  $E_3 = \frac{V_a}{t}$ .

In a static configuration there should now be a balance of stress in the element as

$$\frac{F_a}{A} - d_{33} (c_{33}^E - 2c_{13}^E \nu) \frac{V_a}{t} = 0.$$

If the stack has  $n$  elements, the length of the stack is  $\ell = nt$ . The blocking force developed by the stack can now be found to be

$$F_a = nd_{33}\tilde{k}_a V_a, \quad \tilde{k}_a = \frac{(c_{33}^E - 2c_{13}^E \nu) A}{\ell}, \quad (1)$$

where  $\tilde{k}_a$  can be recognized as the stiffness [N/m] of the stack.

### C. Mechanical model

Fig. 2 shows a simplified schematic of the flexure guided positioning stage. The actuator develops a force that will result in a displacement of the moving platform along the direction indicated.

The mechanical structure is assumed equivalent to a mass-spring-damper system, such as the one given in the mechanical diagram for of Fig. 3. Newton's second law for this system is

$$(M_p + M_a)\ddot{x} = F_a - \tilde{k}_a x - k_f x - c_a \dot{x} - c_f \dot{x}$$

which can be truncated to the form

$$M\ddot{x} + c\dot{x} + kx = F_a,$$

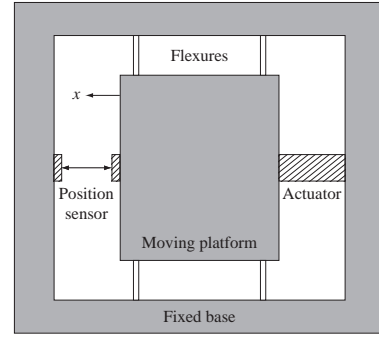


Fig. 2. Simplified schematic of the single degree-of-freedom flexure guided positioning stage.

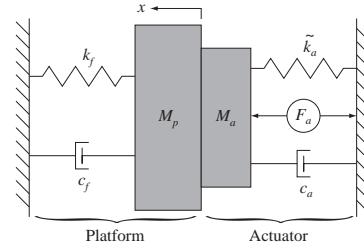


Fig. 3. Mechanical diagram for the positioning stage.

where

$$M = M_p + M_a, \quad c = c_f + c_a, \quad k = k_p + \tilde{k}_a.$$

Using (1), we find the transfer function from applied voltage  $V_a$  to displacement  $x$  to be

$$\hat{G}_{xV_a} = \frac{\hat{x}}{\hat{V}_a} = \frac{nd_{33}\tilde{k}_a}{Ms^2 + cs + k}. \quad (2)$$

### D. Generated charge

Allowing the stack to also move along the 3 axis, we can find the stress  $\sigma_3$  on an element due to a strain  $\epsilon_3$  in this direction according to Hooke's law as

$$\sigma_3 = (c_{33}^E - 2c_{13}^E \nu) \epsilon_3, \quad \nu = \frac{c_{13}^E}{c_{11}^E + c_{12}^E}.$$

The strain of the element is defined as the ratio of the increase in length, or displacement,  $x$ , of the element, and the original length,  $t$ . That is,  $\epsilon_3 = \frac{x}{t}$ .

The generated charge density  $D_3$  on the surfaces of the electrodes due to the stress  $\sigma_3$  and the electric field  $E_3$  is

$$D_3 = d_{33}\sigma_3 + \kappa_{33}^\sigma E_3.$$

The charge produced by an element should be  $q = AD_3$ , thus the charge produced by the stack due to a displacement and an applied voltage should then be

$$q = nd_{33}\tilde{k}_a x + C_p V_a, \quad \tilde{k}_a = \frac{(c_{33}^E - 2c_{13}^E \nu) A}{\ell}, \quad C_p = \frac{n^2 \kappa_{33}^\sigma A}{\ell}, \quad (3)$$

where  $\tilde{k}_a$  is the stack's stiffness as before, and  $C_p$  is the capacitance [F] of the stack.

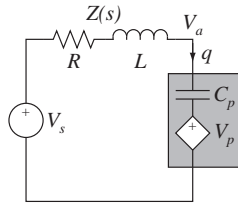


Fig. 4. Circuit with shunt.

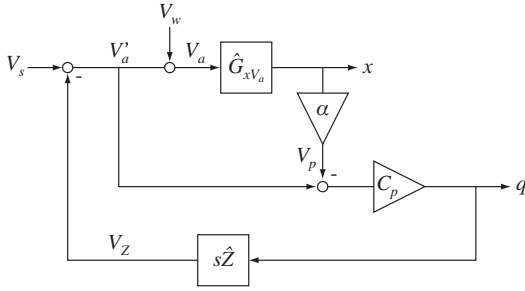


Fig. 5. Block diagram for the shunted system.

The displacement is given by (2), thus the transfer function from applied voltage  $V_a$  to generated charge  $q$  is

$$\hat{G}_{qV_a} = \frac{\hat{q}}{\hat{V}_a} = nd_{33}\tilde{k}_a\hat{G}_{xV_a} + C_p. \quad (4)$$

### E. Shunt

The piezoelectric stack is made from lead zirconate titanate, which is a material with a large dielectric constant. The stack will therefore function as a capacitor. Adding an inductor and a resistor in series with the piezoelectric stack, a series LCR circuit is obtained. This arrangement is shown in Fig. 4.

The loop equation for the circuit in Fig. 4 is

$$V_s = V_Z + V_a,$$

and we can see that the voltage drop over the shunt is

$$\hat{V}_Z = s\hat{Z}q,$$

where the impedance of the shunt  $\hat{Z}$  is

$$\hat{Z} = R + sL,$$

where  $R$  is resistance [ $\Omega$ ] and  $L$  is inductance [H]. The block diagram for the shunted piezoelectric stack can be seen in Fig. 5. From (4) and Fig. 4 we can recognize that  $V_p$  must be

$$V_p = -\frac{nd_{33}\tilde{k}_a}{C_p}x = -\alpha x, \quad \alpha = \frac{nd_{33}\tilde{k}_a}{C_p}.$$

From the block diagram we can find the transfer function from the source voltage  $V_s$  to the applied voltage  $V_a$  to be

$$\hat{G}_{V_aV_s} = \frac{\hat{V}_a}{\hat{V}_s} = \frac{1}{1 + s\hat{Z}\hat{G}_{qV_a}} = \frac{\hat{F}}{1 + \hat{K}\hat{G}_{xV_a}} \quad (5)$$

where

$$\hat{F} = \frac{1}{1 + s\hat{Z}C_p} \quad (6)$$

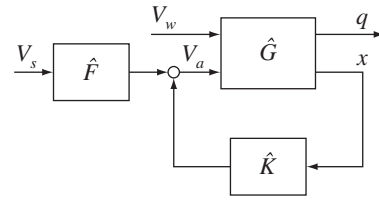


Fig. 6. Feedback control formulation.

and

$$\hat{K} = \frac{s\hat{Z}C_p\alpha}{1 + s\hat{Z}C_p}. \quad (7)$$

From (2) and (4) it is now straight forward to find the transfer function to the displacement and charge as

$$\hat{G}_{xV_s} = \frac{\hat{x}}{\hat{V}_s} = \hat{G}_{xV_a}\hat{G}_{V_aV_s} \quad (8)$$

and

$$\hat{G}_{qV_s} = \frac{\hat{q}}{\hat{V}_s} = \hat{G}_{qV_a}\hat{G}_{V_aV_s}. \quad (9)$$

Shown in the block diagram is a disturbance voltage  $V_w$ , which is added to the applied voltage. The transfer function from disturbance  $V_w$  to applied voltage  $V_a$  can be found to be

$$\hat{G}_{V_aV_w} = \frac{\hat{V}_a}{\hat{V}_w} = \frac{1}{1 + \hat{K}\hat{G}_{xV_a}}, \quad (10)$$

and the transfer function to the displacement  $x$  becomes

$$\hat{G}_{xV_w} = \frac{\hat{x}}{\hat{V}_w} = \frac{\hat{G}_{xV_a}}{1 + \hat{K}\hat{G}_{xV_a}}. \quad (11)$$

In the above development we have introduced the transfer functions  $\hat{F}$  and  $\hat{K}$ . With reference to Fig. 6 we can understand these to be a filter and a feedback controller, respectively. Comparing (5) and (10) we understand that  $\hat{F}$  will filter the source voltage  $V_s$ , such that any reference signal should be filtered by  $\hat{F}^{-1}$ , that is  $\hat{V}_s = \hat{F}^{-1}\hat{r}$ .

## III. EXPERIMENTS

A series of experiments was performed in order to tune the shunt circuit and observe the effectiveness of the proposed technique.

### A. Parameters

For the series LCR circuit, we know that the undamped resonance frequency is given by

$$2\pi f_0 = \frac{1}{\sqrt{LC_p}}. \quad (12)$$

Knowing the resonance frequency of the first vibrational mode of the positioning stage and the capacitance of the piezoelectric stack, the needed inductance necessary for tuning the undamped resonance frequency of the LCR circuit can be found from (12),

$$L = \frac{1}{\sqrt{C_p}(2\pi f_0)^2}. \quad (13)$$

Obtaining experimental gain-phase data for the input  $V_a$  to the outputs  $x$  and  $q$ , it is possible to identify both  $f_0$  and  $C_p$ .

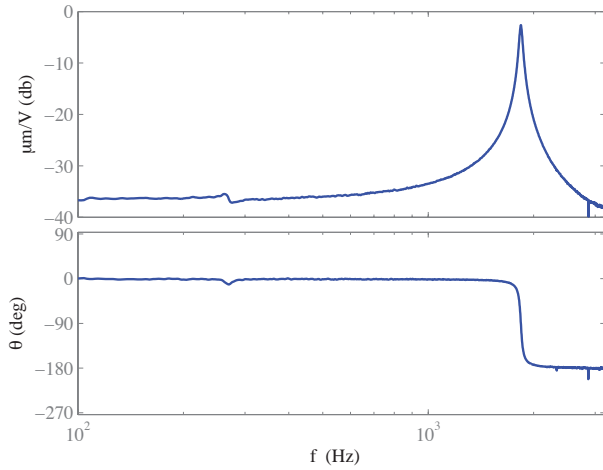


Fig. 7. Measured frequency response from applied voltage  $V_a$  to displacement  $x$ ,  $\hat{G}_{xV_a}$ .

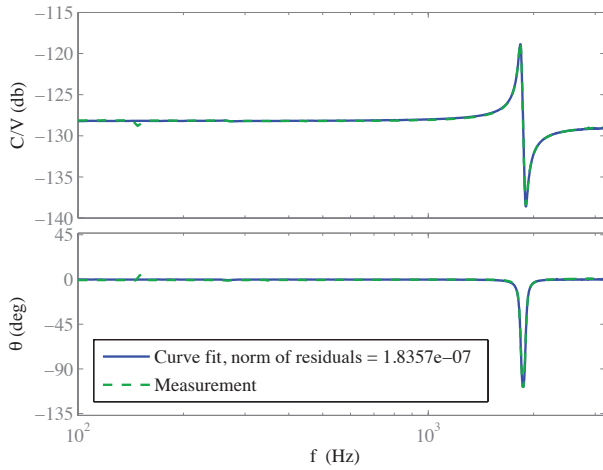


Fig. 8. Measured frequency response from applied voltage  $V_a$  to generated charge  $q$ ,  $\hat{G}_{qV_a}$ , and the curve fit used to identify  $C_p$  and  $\alpha$ . The frequency response from applied voltage  $V_a$  to charge  $q$ ,  $\hat{G}_{qV_a}$ , was generated using the data from Fig. 7 and (4) and compared to the actual measured response.

This was done using a HP356708 Dynamic Signal Analyzer. Inspecting Fig. 7, which displays the response from the applied voltage to displacement,  $f_0$  is found to be 1.84 kHz.

Inspecting (4), it is apparent that the parameters  $C_p$  and  $\alpha = \frac{nd_{33}\bar{k}_a}{C_p}$  can be identified, having obtained experimental data for the transfer functions  $\hat{G}_{xV_a}$  and  $\hat{G}_{qV_a}$ , using e.g. a curve fit. This is shown on Fig. 8. The obtained values are presented in Tab. I<sup>1</sup>.

Now, an estimated value for the required inductance can be found. Using equation (13) the required inductance is 20 mH, which can easily be implemented with a physical inductor. Since the system is not completely without damping, one would expect that the optimal inductance would be slightly

<sup>1</sup>It might be noted that the value for  $C_p$ , using a Fluke 289 multimeter, was found to be 411 nF. The discrepancy between the this value and the value in Tab. I is due to the direct piezoelectric effect  $nd_{33}\bar{k}_a x$  in (3). The applied signal from the multimeter used to determine the capacitance will cause the piezoelectric material to strain, and therefore a larger net charge is measured on electrodes, thus the actual capacitance is overestimated.

TABLE I  
IDENTIFIED PARAMETERS.

$f_0$	1.84 kHz
$C_p$	368 nF
$\alpha$	3.78 MV/m
$R$	57.8 $\Omega$
$L$	19.0 mH

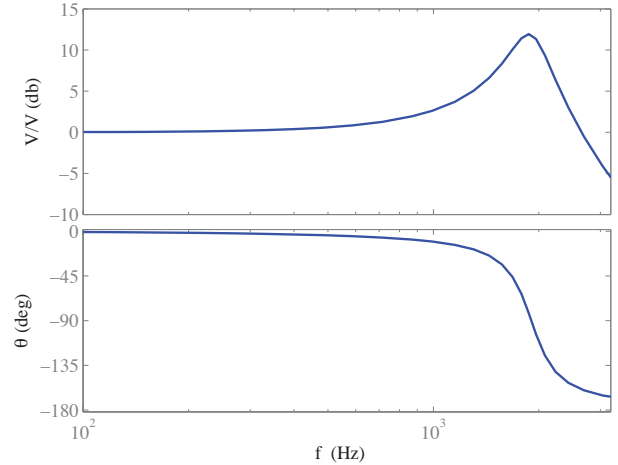


Fig. 9. Computed frequency response of the input filter  $\hat{F}$  using values from Tab. I.

less than the value found using (13).

By minimizing the  $\ell^2$  norm for the expression in (11), using the obtained data for  $\hat{G}_{xV_a}$ ,  $C_p$  and  $\alpha$ , with respect to  $R$  and  $L$ , we should find the values for  $R$  and  $L$  that will minimize the energy of the system. Optimization was performed using `fminsearch` in MATLAB. The obtained values for  $R$  and  $L$  can be found in Tab. I. The value for the the inductance is slightly lower than the one found assuming no damping.

### B. Implementation

The value for the needed inductance suggested that a physically realizable inductor could be used in the shunt. An inductor was constructed using a closed ferrite core and 40 turns of copper wire. A potentiometer was used to implement the required resistance. The inductor and resistor were tuned to their required values using an Agilent LCR Meter E49808. Due to the mechanical limitation in precision, the inductance was set to be 19.5 mH and the resistance set to 58.0  $\Omega$ .

The triangle wave scanning signal and the inverse filter  $F^{-1}$  was implemented on a dSPACE DS1103 using MATLAB and the Real Time Workshop. The actuator was driven by a PiezoDrive PDL200 amplifier. The displacement was measured using a ADE Tech 4810 gage with a ADE Tech 2805 probe. The charge was measured using a 116  $\mu$ F capacitor in series with the shunt and stack. A Tektronix TDS3024B oscilloscope was used to capture the time responses of the positioning stage.

### C. Damping

Adding the shunt  $\hat{Z}$  to the system, using the obtained values for the inductance and the resistance, one would expect

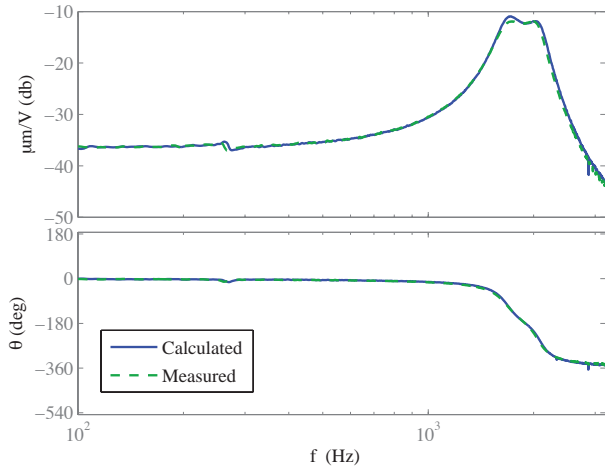


Fig. 10. Measured frequency response from source voltage  $V_s$  to displacement  $x$ ,  $\hat{G}_{xV_s}$ .

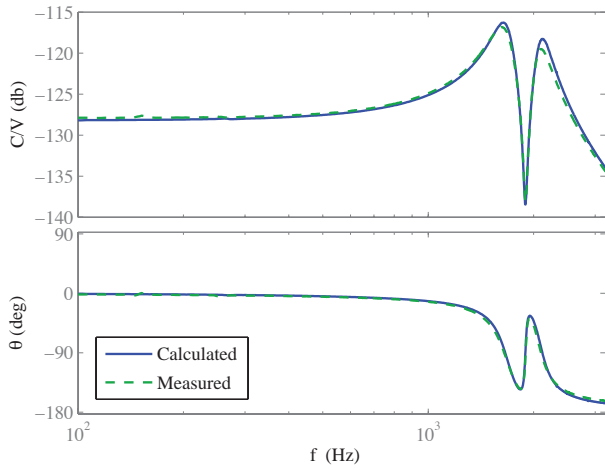


Fig. 11. Measured frequency response from source voltage  $V_s$  to generated charge  $q$ ,  $\hat{G}_{qV_s}$ .

the shunt to attenuate a peak in the transfer function from the supplied voltage  $V_s$  to displacement  $x$ . The calculated response from source voltage to displacement, using data from Fig. 7 and equation (8), is compared to the actual response in Fig. 10. Similarly, the expected response from source voltage  $V_s$  to generated charge  $q$  was found using data from Fig. 7, values from Tab. I and equation (9). The simulated and measured response are compared in Fig. 11. The agreement between the simulated and measured responses supports the modeling technique presented in Section II.

Using the response data for the transfer functions  $\hat{G}_{xV_a}$  and  $\hat{G}_{xV_s}$ , the response for (11) can be calculated, and when compared to the experimental data for (2), the actual damping due to the shunt can be estimated. The result is presented in Fig. 12. Inspecting Fig. 12 the obtained damping can be determined to be 19.6 dB, or equivalently, an attenuation by a factor of 9.55.

#### D. Scanning

Since the source voltage  $V_s$  will be filtered by  $\hat{F}$ , any reference signal applied from the source should compensate

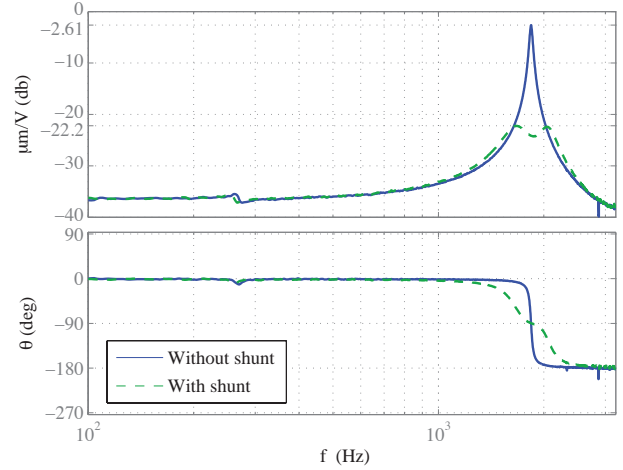


Fig. 12. Estimate of obtained damping. The measured response of  $\hat{G}_{xV_a}$  is compared to the computed response of  $\hat{G}_{xV_a}$ , obtained using the measured response of  $\hat{G}_{xV_s}$  and the inverse of the transfer function  $\hat{F}$ . The difference in maximal magnitude can be seen to be 19.6 dB.

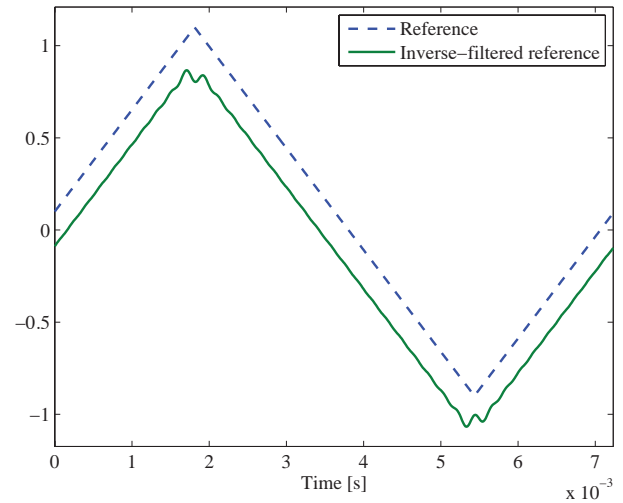


Fig. 13. Triangle wave reference signal, and the signal filtered by  $F^{-1}$ . The signals are offset  $\pm 0.1$  for readability.

for the filter dynamics such that the voltage applied  $V_a$  will be the actual desired reference. The desired input for  $V_a$  and the signal with inverted dynamics  $V_s$  are shown in Fig. 13.

To demonstrate the improvement in scanning performance, two time-series were recorded for two different reference signals. The recorded time-series for the two cases are shown in Figs. 14 and 15. The first time-series in each case shows the open loop response, and the second time-series shows the response when the shunt is present.

We can see from the figures that the shunt circuit significantly reduces unwanted vibrations. It is also apparent that the induced vibrations are larger and the damping more noticeable at a higher fundamental frequency. Some hysteresis can also be observed. The capacitive sensor used is susceptible to some drift, i.e. there is a bias component present in the measurement that vary slowly with time. We have therefore subtracted the mean value in the presented data.

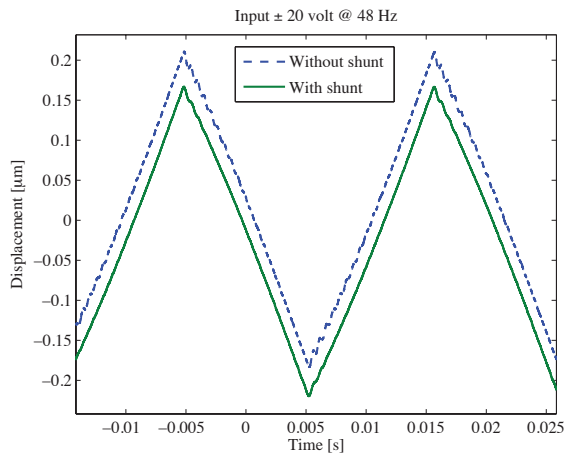


Fig. 14. Response to triangle wave with fundamental frequency at 48 Hz. Signals are compensated for sensor drift (bias) and offset by  $\pm 0.02 \mu\text{m}$  for readability.

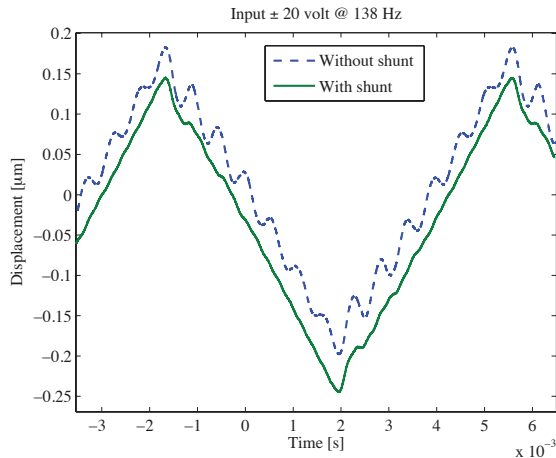


Fig. 15. Response to triangle wave with fundamental frequency at 138 Hz. Signals are compensated for sensor drift (bias) and offset by  $\pm 0.02 \mu\text{m}$  for readability.

#### IV. CONCLUSIONS

Shunt damping, as implemented in this work, has proved to be a simple and effective technique for damping the first mechanical resonance of a piezoelectric stack actuated nanopositioner. The shunt circuit comprised of an inductor and resistor which was straight-forward to implement with passive components. The optimal component values were found using frequency response data and a simple optimization. Experimental results on a high-speed nanopositioner demonstrate a 19.6 dB reduction in the first mechanical resonance. This significantly improves the transient response of the nanopositioner with negligible additional cost or complexity.

#### V. ACKNOWLEDGMENTS

The authors would like to thank Dr. S. O. Reza Moheimani for the opportunity to visit and use the Laboratory for Dynamics and Control of Nanosystems for these experiments, as well as Dr. Kam K. Leang (University of Reno, Nevada) for designing the positioning stage.

#### REFERENCES

- [1] S. Devasia, E. Eleftheriou, and S. O. R. Moheimani, "A survey of control issues in nanopositioning," *IEEE Transactions on Control Systems Technology*, vol. 15, no. 5, pp. 802–823, September 2007.
- [2] Z. Wang, L. Chen, and L. Sun, "An integrated parallel micromanipulator with flexure hinges for optical fiber alignment," in *Proc. IEEE International Conference on Mechatronics and Automation*, Harbin, China, August 2007, pp. 2530–2534.
- [3] B. Potsaid, J. T. Wen, M. Unrath, D. Watt, and M. Alpay, "High performance motion tracking control for electronic manufacturing," *Journal of Dynamic Systems, Measurement, and Control*, vol. 129, pp. 767–776, November 2007, mirror Scanner.
- [4] D. Y. Abramovitch, S. B. Andersson, L. Y. Pao, and G. Schitter, "A tutorial on the mechanisms, dynamics, and control of atomic force microscopes," in *Proc. American Control Conference*, New York City, NY, July 2007, pp. 3488–3502.
- [5] A. A. Tseng, S. Jou, A. Notargiacomo, and T. P. Chen, "Recent developments in tip-based nanofabrication and its roadmap," *Journal of Nanoscience and Nanotechnology*, vol. 8, no. 5, pp. 2167–2186, May 2008.
- [6] T. Ando, N. Kodera, T. Uchihashi, A. Miyagi, R. Nakakita, H. Yamashita, and K. Matada, "High-speed atomic force microscopy for capturing dynamic behavior of protein molecules at work," *e-Journal of Surface Science and Nanotechnology*, vol. 3, pp. 384–392, December 2005.
- [7] G. Schitter, K. J. Åström, B. E. DeMartini, P. J. Thurner, K. L. Turner, and P. K. Hansma, "Design and modeling of a high-speed AFM-scanner," *IEEE Transactions on Control Systems Technology*, vol. 15, no. 5, pp. 906–915, September 2007.
- [8] A. D. L. Humphris, M. J. Miles, and J. K. Hobbs, "A mechanical microscope: high-speed atomic force microscopy," *Applied Physics Letters*, vol. 86, pp. 034 106(1–3), 2005.
- [9] M. J. Rost, L. Crama, P. Schakel, E. van Tol, G. B. E. M. van Velzen-Williams, C. F. Overgaw, H. ter Horst, H. Dekker, B. Okhuijsen, M. Seynen, A. Vijftigschild, P. Han, A. J. Katan, K. Schoots, R. Schumm, W. van Loo, T. H. Oosterkamp, and J. W. M. Frenken, "Scanning probe microscopes go video rate and beyond," *Review of Scientific Instruments*, vol. 76, no. 5, pp. 053 710(1–9), April 2005.
- [10] J. L. Fanson and T. K. Caughey, "Positive position feedback control for large space structures," *AIAA Journal*, vol. 28, no. 4, pp. 717–724, 1990.
- [11] S. S. Aphale, B. Bhikkaji, and S. O. R. Moheimani, "Minimizing scanning errors in piezoelectric stack-actuated nanopositioning platforms," *IEEE Transactions on Nanotechnology*, vol. 7, no. 1, pp. 79–90, January 2008.
- [12] A. J. Fleming and S. O. R. Moheimani, "Sensorless vibration suppression and scan compensation for piezoelectric tube nanopositioners," *IEEE Transactions on Control Systems Technology*, vol. 14, no. 1, pp. 33–44, January 2006.
- [13] A. J. Fleming, S. Behrens, and S. O. R. Moheimani, "Optimization and implementation of multi-mode piezoelectric shunt damping systems," *IEEE/ASME Transactions on Mechatronics*, vol. 7, no. 1, pp. 87–94, March 2002.
- [14] A. Sebastian, A. Pantazi, S. O. R. Moheimani, H. Pozidis, and E. Eleftheriou, "A self servo writing scheme for a MEMS storage device with sub-nanometer precision," in *Proc. IFAC World Congress*, Seoul, Korea, July 2008, pp. 9241–9247.
- [15] S. S. Aphale, A. J. Fleming, and S. O. R. Moheimani, "Integral control of resonant systems with collocated sensor-actuator pairs," *IOP Smart materials and Structures*, vol. 16, pp. 439–446, April 2007.
- [16] A. J. Fleming, S. S. Aphale, and S. O. R. Moheimani, "A new method for robust damping and tracking control of scanning probe microscope positioning stages," *IEEE Transactions on Nanotechnology*, In Press, 2009.
- [17] B. Bhikkaji and S. O. R. Moheimani, "Integral resonant control of a piezoelectric tube actuator for fast nanoscale positioning," *IEEE/ASME Transactions on Mechatronics*, vol. 13, no. 5, pp. 530–537, October 2008.
- [18] K. K. Leang and A. J. Fleming, "High-speed serial-kinematic AFM scanner: design and drive considerations," *Asian Journal of Control*, vol. 11, no. 2, pp. 144–153, March 2009.